Inorganic Chemistry

pubs.acs.org/IC Article

An NADH-Inspired Redox Mediator Strategy to Promote Second-Sphere Electron and Proton Transfer for Cooperative Electrochemical CO_2 Reduction Catalyzed by Iron Porphyrin

Peter T. Smith, Sophia Weng, and Christopher J. Chang*

Cite This: https://dx.doi.org/10.1021/acs.inorgchem.0c01162 Read Online

ABSTRACT: We present a bioinspired strategy for enhancing electrochemical carbon dioxide reduction catalysis by cooperative use of base-metal molecular catalysts with intermolecular second-sphere redox mediators that facilitate both electron and proton transfer. Functional synthetic mimics of the biological redox cofactor NADH, which are electrochemically stable and are capable of mediating both electron and proton transfer, can enhance the activity of an iron porphyrin catalyst for electrochemical reduction of CO_2 to CO, achieving a 13-fold rate improvement without altering the intrinsic high selectivity of this catalyst platform for CO_2 versus proton reduction. Evaluation of a systematic series of NADH analogues and redox-inactive control additives with varying proton and electron reservoir properties reveals that both electron and proton transfer contribute to the observed catalytic enhancements. This work establishes that second-sphere dual control of electron and proton inventories is a viable design strategy for developing more effective electrocatalysts for CO_2 reduction, providing a starting point for broader applications of this approach to other multielectron, multiproton transformations.

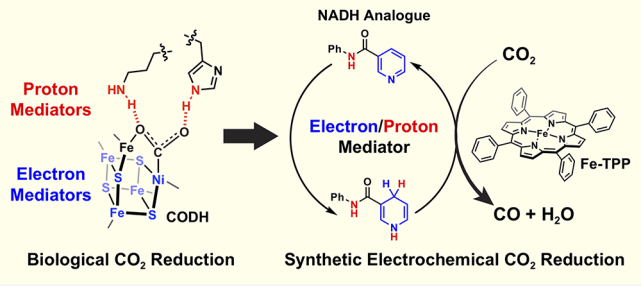

■ INTRODUCTION

Catalyzing the CO_2 reduction reaction by electrochemical means offers an approach for converting this greenhouse gas into value-added chemical products with sustainable energy input.[1−15] Efforts in molecular electrocatalysts for CO_2 reduction have predominantly focused on the two-electron/two-proton reduction of CO_2 into CO, which can then be fed into numerous existing industrial processes for chemical synthesis. Iron porphyrins, in particular, have been the subject of extensive research owing to their high selectivity for CO_2 versus proton reduction, structural tunability, and compatibility with various electrolyte media.[16−24] Beyond this platform and other privileged primary coordination sphere motifs, approaches to enhance CO_2 reduction catalysis with secondary coordination sphere pendants have largely focused on improving the delivery of protons using intramolecular proton relays and/or stabilization of metal-bound CO_2 intermediates via hydrogen bonding.[17,18,25−39] Additionally, reduced CO_2 intermediates can be captured by inter/intramolecular Lewis acid cations[40−42] or intramolecular charge-compensation moieties, such as ammonium[21,43] or imidazolium groups.[44−46]

In addition to proton control, strategies for facilitating electron delivery from the secondary coordination sphere for CO_2 reduction have also been explored. One elegant example from Shafaat's laboratory embeds nickel cyclam, a classic CO_2 reduction catalyst, within a blue copper protein that acts as an outer-sphere electron reservoir to enhance activity.[47] We have also shown that reticular materials can influence CO_2 selectivity and activity by electronic delocalization in the secondary coordination sphere.[48,49] Redox-active ligands based on polypyridines,[50−55] imines,[56] and porphyrins[57,58] can also be employed for CO_2 reduction, where ligand-centered reductions offer the advantage of removing electron density away from the metal center to diminish metal hydride formation and off-pathway H_2 evolution.[59,60] Our laboratory and Miller's laboratory have identified molecular terpyridine-based iron complexes that are highly active CO_2-to-CO electrocatalysts that operate at extremely low overpotentials due to electronic delocalization.[54,55] Finally, bulk electron transfer can be improved by electrode surface attachment.[61−65]

Against this backdrop of literature showing benefits of either second-sphere proton or electron control for electrochemical CO_2 reduction catalysis, we sought to develop a second-sphere approach that enables dual management of both electron *and* proton inventories. Our synthetic efforts are inspired by

Received: April 20, 2020

Scheme 1. Bioinspired Design of Second-Sphere Additives That Enable Dual Electron and Proton Control for Facilitating Electrochemical CO_2 Reduction Catalyzed by Iron Tetraphenylporphyrin (Fe-TPP)

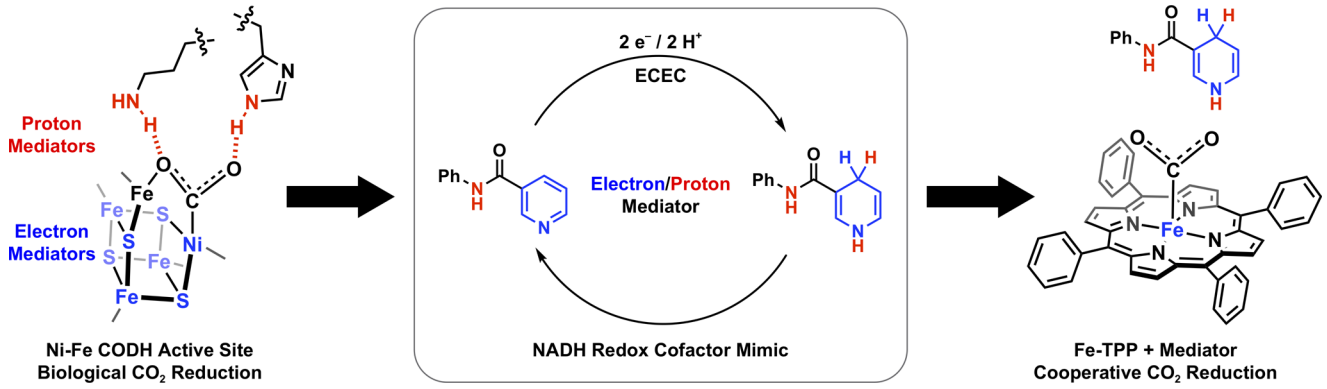

biological CO_2 reduction enzymes. Included are carbon monoxide dehydrogenases (CODH)[66] and formate dehydrogenases[67] that couple primary active sites with properly positioned second-sphere proton relays and electron reservoirs to enable catalysis near thermodynamic potentials (Scheme 1). Such enzymes can be utilized for electrochemical CO_2 reduction,[68,69] but challenges associated with direct electron transfer from electrodes to buried active sites within these macromolecules in the absence of their native redox partners in the cell require the addition of small-molecule redox mediators like ferrocenes, viologens, and quinones.[70,71] To pursue such biology-to-chemistry concept transfer, we turned to the use of organic cofactors such as nicotinamide adenine dinucleotide (NAD^+/NADH) that can facilitate both electron and proton transfer. However, NADH and various synthetic organic analogues are often incompatible with electrochemically driven catalytic cycles due to formation of radical intermediates leading to decomposition.[72] As such, we sought to overcome this challenge by judicious choice of catalyst and electron−proton mediator components with matched reduction potentials to avoid these off-cycle decomposition pathways.

In this report, we present a cooperative electrochemical CO_2 reduction strategy that combines a base-metal molecular catalyst in the primary coordination sphere with intermolecular NADH-like redox mediators that facilitate electron and proton transfer from the secondary coordination sphere (Scheme 1). We chose *N*-phenylnicotinamide (**1**) as a dual electron−proton mediator that possesses a basic pyridine and promotes two-electron/two-proton transfer pathways, coupled to the classic iron tetraphenylporphyrin (**Fe-TPP**) electrocatalyst system for CO_2 reduction. As reduction of pyridine heterocycles can give 1,2- or 1,4-dihydropyridine regioisomers,[73] we exploited this property to evaluate the *N*-phenylisonicotinamide (**2**) isomer as an additional electron−proton mediator. When added in catalytic amounts, both **1** and **2** significantly enhance CO formation during electrochemical CO_2 reduction catalyzed by **Fe-TPP** with up to a 13-fold improvement in catalytic activity without sacrificing CO_2 versus proton substrate selectivity. Further studies with a systematic series of control additives reveals that both proton and electron reservoir capacities contribute to the observed second-sphere driven improvements in electrochemical CO_2 reduction efficiency. This work provides a starting point for designing catalysts for a broader range of multielectron, multiproton transformations with second-sphere additives or pendants that can manage both electron and proton inventories.

RESULTS AND DISCUSSION

NADH Analogues Show Enhanced Current Activity in the Presence of External Proton Sources. We initiated our studies by evaluating the electrochemical behavior of NADH analogues in the presence of external proton sources with the goal of developing electron−proton redox mediators with multielectron, multiproton capabilities and electrochemical stability. As a starting point, the cyclic voltammogram (CV) of **1** under a N_2 atmosphere in anhydrous DMF electrolyte shows an irreversible reduction with a peak potential at −2.52 V vs Fc/Fc^+ (Figure 1). This result suggests an EC mechanism, in

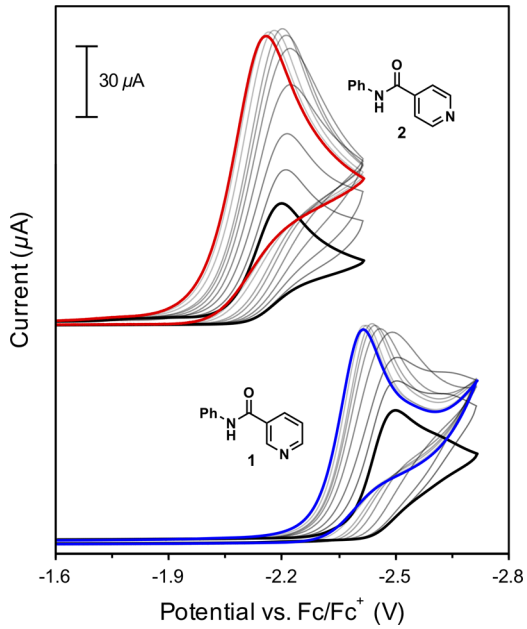

Figure 1. Cyclic voltammograms of 5 mM NADH analogues **1** (blue) and **2** (red) in 0.1 M $TBAPF_6$ DMF electrolyte under a N_2 atmosphere with titration of 0−100 mM phenol. Scan rate = 100 mV/s.

which the one-electron reduced species undergoes a rapid chemical reaction. The CV of the isomeric analogue **2** shows a similar EC wave but at a more positive peak potential of −2.21 V. Upon titration of phenol as a proton source into the solution of **1** or **2** under a N_2 atmosphere, we observe a positive shift in peak potential and concomitant increase in peak current in a dose-dependent manner until a saturation

https://dx.doi.org/10.1021/acs.inorgchem.0c01162
Inorg. Chem. XXXX, XXX, XXX−XXX

level is reached above 5 equiv of added phenol. The peak potentials for **1** and **2** in the presence of excess phenol are −2.40 and −2.14 V, respectively. Integration of the reduction waves for **1** and **2** in the absence of phenol gives 29.8 and 29.6 μC of charge, respectively, whereas in the presence of 100 mM phenol, electrochemical reductions of **1** and **2** consume 63.0 and 72.6 μC, respectively. These data suggest a transition from a one-electron to a two-electron reduction process with added acid, which is reminiscent of the ECEC mechanism that is classically observed for quinone species in the presence of proton sources.[74] We speculate that hydrogen bonding between the basic pyridine nitrogen and acidic phenol triggers the positive shift in onset potential, and protonation after the initial one-electron reduction step produces a species that is more easily reduced than **1**, so an overall two-electron/two-proton reduction process is facilitated as more phenol is added. This reaction leads to the proposed dihydropyridines **1′** and **2′** as shown in Scheme 2. A new oxidation wave is also observed

Scheme 2. Reductions of NADH Analogues 1 and 2 Produce the Corresponding 1,4-Dihydropyridines, 1′ and 2′

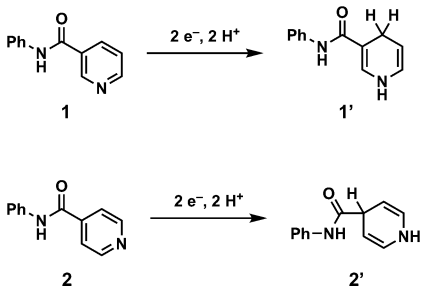

at −0.61 V for **1** and at −0.24 V for **2** (Figures S1−S3), indicative of oxidation of the incipient dihydropyridine intermediate. After titration of 5 equiv of phenol, the CVs show complete conversion to an ECEC mechanism, establishing the potential for NADH analogues **1** and **2** in the presence of complementary acid sources to act as two-electron/two-proton mediators while also tuning redox potentials to more positive potentials.

CVs of the structurally similar *N*-phenylpicolinamide (**3**) exhibits a similar ECEC-type wave upon phenol titration with a peak potential of −2.33 V (Figure S3). Interestingly, unsubstituted nicotinamide exhibits different behavior with CVs revealing a more negative reduction potential of −2.57 V in the presence of 100 mM phenol and a peak area that does not double as expected for a two-electron process, suggesting an undesired reduction mechanism (Figure S7). The ECEC behavior observed in CVs of additives **1**−**3** with an added proton source remains unchanged up to 500 mM phenol in both N_2 and CO_2 saturated electrolyte (Figures S8−S10). Taken together, these observations establish that these synthetic NADH analogues can serve as two-electron/two-proton reservoirs in the presence of a complementary proton source and that the reduced additives neither behave as CO_2 reduction nor proton reduction electrocatalysts on the CV time scale.

Controlled Potential Electrolysis Experiments on NADH Analogues Provide Evidence for Dihydropyridine Formation. To provide further evidence to support the two-electron behavior in these synthetic NADH analogues, we performed controlled potential electrolysis (CPE) on 5 mM solutions of **1** and **2** at −2.4 V vs Fc/Fc$^+$ with 500 mM phenol under a CO_2 atmosphere. The CPE data show that the overall charge consumed is close to the two electrons per molecule stoichiometry that would theoretically yield the reduced dihydropyridines **1′** or **2′**, respectively (Figure 2). The

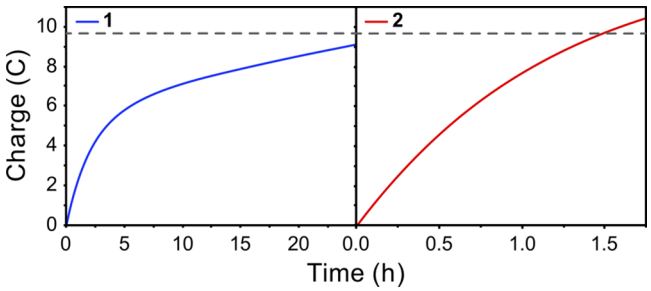

Figure 2. Controlled potential electrolyses showing charge consumption of 5 mM NADH analogues **1** (blue) and **2** (red) at −2.4 V vs Fc/Fc$^+$ in 0.1 M $TBAPF_6$ DMF electrolyte containing 500 mM phenol under a CO_2 atmosphere. The gray dashed line denotes the charge required for complete two-electron reduction of **1** and **2**.

catholyte consisted of 10 mL of 5 mM solutions of each additive, which would require 9.6 C for a complete two-electron reduction. Electrolysis of **1** led to rapid charge consumption during the first 5 h but then required over 25 h of electrolysis for complete reduction (Figure 2). This behavior is likely due to low current density at this applied potential, which is at the peak potential for the reduction of **1** (Figure 1). Notably, more negative applied potentials were avoided to minimize background hydrogen evolution at the glassy carbon electrode. In contrast, **2** is fully reduced after 1.5 h of electrolysis, quickly consuming a full 9.6 C as a result of the more positively shifted reduction potential of **2** relative to **1**, where the electron-withdrawing group of the former is now located on the 4-position. The applied potential of −2.4 V is now 260 mV more negative than the peak potential for the reduction of **2** so that the rate of reduction of **2** is primarily limited by diffusion, whereas reduction of **1** is limited by diffusion as well as electron transfer. We attribute the slight excess of charge consumed to background hydrogen evolution, which was detected by gas chromatography (GC). No reduced carbon products were detected, confirming that the electrochemically generated dihydropyridines do not directly react with CO_2, as has been observed in other organohydride systems.[75] Indeed, the hydricity values of a range of substituted dihydropyridines have been reported and are not strong enough to reduce CO_2 into formate.[76]

We also performed a direct chemical reduction of **1** using $LiAlH_4$ with an anaerobic aqueous workup to give **1′**. ESI mass spectrometry shows an *m*/*z* increase of 2, consistent with dihydropyridine formation. Moreover, the UV/vis absorption spectrum of starting additive **1** shows a single absorption at 250 nm, but spectra of the products of both chemical and electrochemical reduction of **1** show the same prominent absorption band at 355 nm (Figure 3A). Interestingly, this absorption behavior is similar to that of NAD$^+$/NADH,[77] suggesting a similar change to the aromatic pyridine π system in this synthetic analogue. Furthermore, the ^{1}H NMR spectrum of chemically synthesized **1′** shows nearly complete consumption of starting material and the formation of new peaks at 3.10, 4.56, 5.94, and 7.08 ppm consistent with allylic and vinylic protons in the proposed dihydropyridine structure

https://dx.doi.org/10.1021/acs.inorgchem.0c01162
Inorg. Chem. XXXX, XXX, XXX−XXX

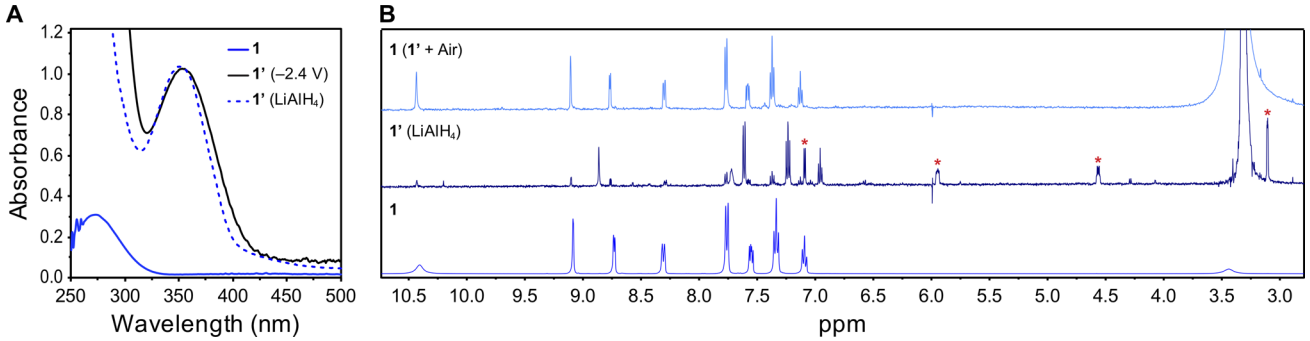

Figure 3. (A) Overlaid UV/vis spectra in DMF solution of **1** (solid blue) and **1′** synthesized by either chemical reduction with $LiAlH_4$ (dashed blue) or by electrochemical reduction at −2.4 V in the presence of excess phenol (black). (B) Overlaid ^1H NMR spectra in DMSO-d_6 of **1** and **1′** synthesized by chemical reduction with $LiAlH_4$ and **1** obtained by oxidation of **1′** upon exposure to air. Peaks labeled with asterisks are assigned to the newly formed allylic and vinylic protons. Peaks between 3.3 and 3.5 ppm are assigned to residual water.

(Figure 3B). Full peak assignment is provided in Figure S14. Exposure of **1′** to air leads to rapid reformation of **1** as observed by ^1H NMR, indicating the reversible redox nature of this additive.

Synthetic NADH Analogues Promote Higher Catalytic Current for Iron Porphyrin in the Presence of CO_2. We next tested the ability of **1** to act as an electron−proton transfer mediator for the CO_2 reduction reaction catalyzed by **Fe-TPP**. The peak reduction potentials for **1** and **2** in the presence of excess phenol are −2.40 and −2.14 V, respectively, which lie in the same range as the formal Fe^I/Fe^0 reduction at −2.15 V with **Fe-TPP** where CO_2 reduction occurs.[16] Titration of phenol into a DMF electrolyte solution of **Fe-TPP** saturated with CO_2 shows the expected significant increase in catalytic current with peak shaped waves indicative of fast catalysis (Figure S15). We then repeated this CV experiment with the addition of either 1 or 5 equiv of additives **1** and **2** (Figures S16−S19). At low concentrations of phenol, the reductions of **1** and **2** are clearly observable in the range of the catalytic CO_2 reduction wave. Figure 4 shows the overlaid CV traces at the highest phenol concentration of 500 mM with the catalytic currents normalized to the one-electron peak height for the formal Fe^{II}/Fe^I reduction of **Fe-TPP**, i_p^0. With 1 equiv of **1**, a modest increase in peak catalytic current is observed at −2.25 V relative to **Fe-TPP** alone. However, **1** has a peak reduction potential of −2.40 V under these conditions,

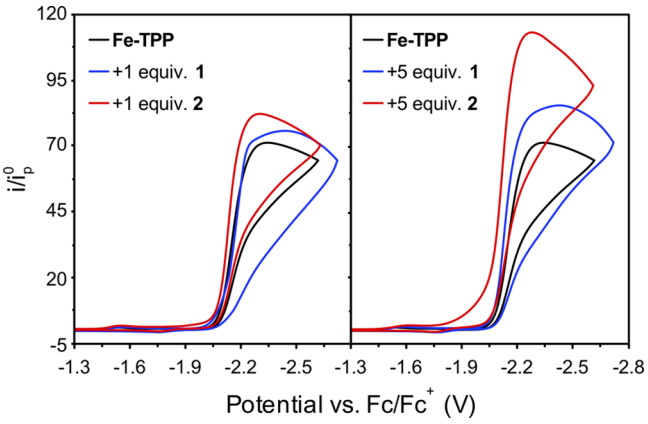

Figure 4. CVs of **Fe-TPP** (black) in the presence of 1 or 5 equiv of additives **1** (blue) or **2** (red) in 0.1 M $TBAPF_6$ DMF electrolyte containing 500 mM phenol under a CO_2 atmosphere. Current is normalized to the formal Fe^{II}/Fe^I reduction of **Fe-TPP**, i_p^0.

which is reflected by a larger difference in catalytic current with added **1** at more negative potentials in Figure 4. In contrast, additive **2** has a peak reduction potential of −2.14 V under these conditions, which more closely matches where **Fe-TPP** catalyzes CO_2 reduction. This redox matching results in a more significant increase in peak catalytic current in the presence of 1 equiv of NADH analogue **2** compared to **1**, with further amplification in the presence of 5 equiv of additive. Taken together, these results suggest that additives **1** and **2** can participate as cocatalysts with **Fe-TPP** for cooperative electrochemical CO_2 reduction.

Controlled Potential Electrolysis Experiments Confirm That NADH Analogues Enhance Electrochemical CO_2 Reduction Catalyzed by Iron Porphyrin. We then performed CPE experiments to quantify product formation for electrochemical CO_2 reduction reactions catalyzed by **Fe-TPP** in the absence or presence of the NADH analogues **1** and **2** in addition to a broader set of NADH mimics (Scheme 3). CPE

Scheme 3. Chemical Structures of Synthetic NADH-Type Additives 1−7

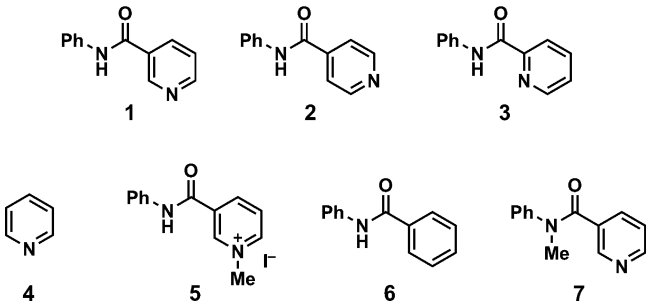

experiments were conducted with 0.5 mM **Fe-TPP**, 0.5 mM additive, and 500 mM phenol under CO_2 for 16 h at −2.4 V vs Fc/Fc^+. Charge accumulation over time is plotted in Figure 5, and a summary of the data is listed in Table 1. With no additive, 4.9 mL of CO was generated. In comparison, addition of 1 equiv of **1** yielded over 3 times as much CO under the same conditions, establishing the ability for **1** to increase the catalytic activity of **Fe-TPP** for CO_2 reduction. Moreover, addition of 1 equiv of **2** yields 3.7 times as much CO as **Fe-TPP** alone, highlighting the redox tunability of these nicotinamide additives. Additive **3** yields a similar increase in CO production. Current density over time is plotted in Figure S22, showing that the current for each experiment drops

https://dx.doi.org/10.1021/acs.inorgchem.0c01162
Inorg. Chem. XXXX, XXX, XXX−XXX

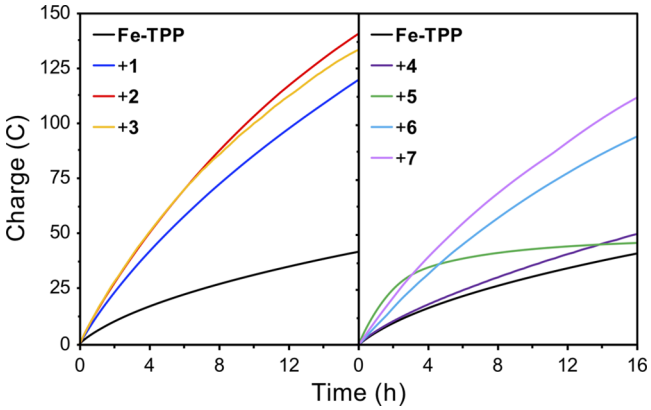

Figure 5. CPEs of 0.5 mM **Fe-TPP** in the presence of 1 equiv of additives **1**−**7** in 0.1 M $TBAPF_6$ DMF electrolyte containing 500 mM phenol under CO_2 performed at −2.4 V vs Fc/Fc^+.

Table 1. CPE Data Summarizing Effects of NADH-Type Additives on Electrochemical CO_2 Reduction Catalyzed by Iron Porphyrin

catalysts	charge (C)	vol. CO (mL)[b]	FE_{CO} (%)[b]	avg. j_{CO} (mA cm^{-2})[c]	TOF_{max} (s^{-1})[d]
Fe-TPP	41.8	4.9	93	0.67	5.24×10^4
+1	119.2	15.0	86	2.07	5.00×10^5
+2	141.0	17.9	108	2.45	7.01×10^5
+3	132.7	16.8	87	2.31	6.23×10^5
+4	50.4	6.0	94	0.82	7.85×10^4
+5	46.0	5.4	92	0.74	6.39×10^4
+6	94.5	11.9	104	1.63	3.10×10^5
+7	112.5	14.2	100	1.95	4.44×10^5

[a]CPEs performed with 0.5 mM **Fe-TPP**, with or without a 0.5 mM concentration of the synthetic NADH analogue as an additive, at a potential of −2.4 V vs Fc/Fc^+ in 0.1 M $TBAPF_6$ DMF electrolyte containing 500 mM phenol under a CO_2 atmosphere for 16 h. [b]Determined using gas chromatography equipped with a flame ionization detector and a known calibration curve. Faradaic efficiency (FE) values are estimated to have an error of ±10%. [c]Determined by averaging the observed current density during each 16 h electrolysis experiment and multiplying by the FE_{CO}. [d]Estimated from the average j_{CO} during each electrolysis (see Supporting Information).

significantly over the long-term CPE experiments, which may be due to the relatively negative applied potential of −2.4 V that accelerates catalyst decomposition. All experiments revealed CO to be the major product accounting for approximately 90−100% Faradaic efficiency (FE), consistent with the high selectivity for iron porphyrin catalysts, and showed that these cooperative electron−proton redox mediators improved catalytic activity without sacrifices in catalytic selectivity.[16,18,23,24] Indeed, only trace amounts of H_2 were detected by GC (Table S1), and no liquid products were detected by ^1H NMR spectroscopy. Noting that some dihydropyridines may be capable of reducing CO_2 into formate via hydride transfer,[78] the formation of CO as the sole reduced carbon product in this system suggests a different mechanism for enhanced electron and proton transfer with catalysis occurring at **Fe-TPP**. Along these lines, an elegant related study by Anson and Stahl showed an increase in current density for reduction of O_2 into H_2O_2 and H_2O using quinones as electron−proton mediators.[79] Similarly, aminoxyl radicals can aid in electron−proton transfer for catalytic electrochemical oxidations.[80]

The observed rate constants (k_{obs}) can be estimated from the CO-specific current densities (j_{CO}), since the charge consumed is directly associated with catalyst turnover.[81] The common foot-of-the-wave analysis determining rate constants from CV traces is not applicable in this system, because the reduction of **1** occurs more negative than the **Fe-TPP** foot-of-the-wave, whereas the reduction of **2** occurs more positive than the **Fe-TPP** foot-of-the-wave, which obscures this type of analysis. As such, we used the average j_{CO} from direct product detection and quantification with the assumption that the redox mediator did not change the rate-determining step for **Fe-TPP** catalysis as product distributions were identical with and without the additive. Using this method, the maximum turnover frequency ($TOF_{max} = k_{obs}$) for 0.5 mM **Fe-TPP** under CO_2 in the presence of 500 mM phenol was estimated to be 5.24×10^4 s^{-1}, which is in agreement with literature reports under conditions of large proton excess.[21,36,45,81] In the presence of 1 equiv of **1** or **2**, patent increases in the **Fe-TPP** TOF_{max} are observed with estimated values of 5.00×10^5 and 7.01×10^5 s^{-1}, respectively. These values correspond to 9.5- and 13.4-fold increases in rate, respectively. Catalytic Tafel plots could then be constructed to visualize the relationship between TOF and overpotential.[81] Figure 6 depicts the Tafel

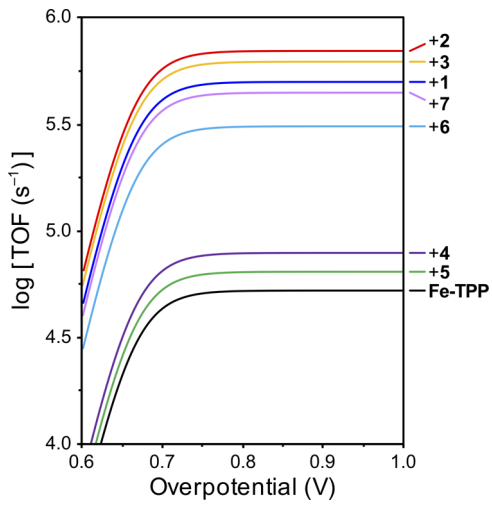

Figure 6. Catalytic Tafel plots for **Fe-TPP** in the absence or presence of 1 equiv of NADH mimics **1**−**7** derived from the k_{obs} values estimated from controlled potential electrolysis experiments.

plots for **Fe-TPP** in the absence and presence of synthetic NADH analogues **1** and **2**, further demonstrating the substantial rate enhancement for CO production by **Fe-TPP** in the presence of these two additives.

We next expanded these studies to the broader set of NADH mimics to decipher contributions of electron and proton relays in a systematic fashion (Scheme 3). First, pyridine additive **4** was tested to probe the role of the basic nitrogen atom in the observed catalytic enhancements. It has previously been hypothesized that pyridine additives can coordinate to cobalt phthalocyanine catalysts to increase their nucleophilicity and CO_2 reduction activity.[82] However, CPE of **Fe-TPP** with 1 equiv of **4** does not show a significant increase in charge consumption and CO production (Figure 5 and Table 1) relative to **Fe-TPP** alone. Second, the methylated pyridinium additive **5**, a closer structural mimetic of NAD^+, was used to determine the importance of the ECEC mechanism, because

https://dx.doi.org/10.1021/acs.inorgchem.0c01162
Inorg. Chem. XXXX, XXX, XXX−XXX

this charged pyridinium undergoes two stepwise reductions, the first of which is proton-independent (Figure S5). CPE of **Fe-TPP** with 1 equiv of **5** shows a similarly high rate of charge consumption and current density as observed with additives **1**−**3** (Figures 5 and S22). However, after this initial increase, the catalytic current decreases dramatically, and the cumulative CO production is comparable to that of **Fe-TPP** alone, which we attribute to the formation of radical anions that dimerize or decompose catalyst. Figure 6 further shows that the log(TOF)−overpotential relationship for **Fe-TPP** is not significantly changed upon addition of **4** or **5**.

Additional synthetic NADH analogues were then investigated as additives to probe contributions of second-sphere electron and proton relays to enhanced CO_2 catalysis. CPE experiments were performed using benzanilide **6** as a redox-inactive additive that retains the amide substituent. Previous work from our laboratory demonstrated that intramolecular amide pendants can significantly enhance the reduction of CO_2 to CO with proper second-sphere positioning.[29] In agreement with that study, the CPE experiments performed with **Fe-TPP** and 1 equiv of **6** lead to improved rates of CO production (5.9-fold increase) but not to the levels achieved with additives **1**−**3** seen in Figure 6 that possess both electron and proton transfer capabilities (9.5- to 13.4-fold rate increases). Indeed, CVs of **6** in the presence of phenol do not show the ECEC behavior observed with additives **1**−**3**. Instead, a catalytic wave is observed with a peak area that more than triples with increasing phenol concentration, indicating that additive **6** behaves solely as a proton source through the amide NH moiety (Figure S6). Finally, we tested pyridine amide additive **7**, where the amide nitrogen atom is methylated to remove benefits of hydrogen bonding and/or proton relays but retains the redox-active reservoir. As observed with proton-only **6**, electron-only additive **7** increases charge consumption and rates of CO production compared to **Fe-TPP** alone (8.4-fold) but not to the same extent as NADH analogues **1**−**3** that have the capacity for both electron and proton management (Figures 6 and Figure S24). Interestingly, the enhanced catalysis with additive **1** is not simply a summation of the benefits provided by hydrogen bonding or proton donation with **6** and by electron transfer with **7**, suggesting a more complex interplay. Nevertheless, these data suggest the participation of both electron and proton relay components in enhancing electrochemical CO_2 reduction catalysis, as NADH analogues that possess dual electron−proton redox reservoir capabilities are superior to additives that only have either electron or proton transfer capacity.

Finally, as NADH analogue **2** showed the highest activity enhancements for electrochemical CO_2 reduction, we performed further dose-dependent CPE experiments with this additive. Figure 7 compares relative current density and charge accumulation values during 1 h of electrolysis at −2.4 V with **Fe-TPP** under a CO_2 atmosphere and 0, 1, 5, 10, or 15 equiv of additive **2**. Addition of 1 equiv of **2** leads to a significant enhancement in average current density to 4.19 mA/cm^2, compared to 1.64 mA/cm^2 with **Fe-TPP** alone. However, increasing doses of **2** to 5, 10, or 15 equiv provides only a modest further current density enhancement. We speculate that this saturation behavior could be due to inherent rate limitations of the parent **Fe-TPP** catalysis and/or insufficient electrolysis to reduce enough **2** to couple to **Fe-TPP** to be effective in the catalytic cycle, as the two components must interact intermolecularly. Further experiments beyond the scope of this work are required to elucidate such complex mechanistic details.

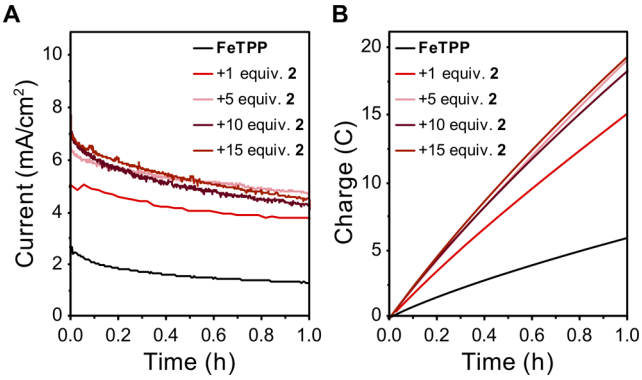

Figure 7. CPEs of 0.5 mM **Fe-TPP** in the presence of 0−15 mM additive **2** in 0.1 M $TBAPF_6$ DMF electrolyte containing 500 mM phenol under a CO_2 atmosphere plotting (A) current density and (B) charge accumulation over a period of 1 h at −2.4 V vs Fc/Fc$^+$.

■ CONCLUDING REMARKS

In summary, we have presented a strategy for enhancing electrochemical CO_2 reduction catalysis through the use of second-sphere additives that have dual electron−proton reservoir capabilities. We establish this concept using synthetic NADH analogues as electron−proton mediators with the molecular CO_2 reduction catalyst **Fe-TPP**. Indeed, although extensive efforts have provided valuable design strategies for facilitating second-sphere proton transfer for electrochemical CO_2 reduction, our findings show that such electrocatalysts can be further augmented by adding electron transfer relays as well. Specifically, the NADH-inspired nicotinamide-based additives **1**−**3** undergo an ECEC reduction pathway to subsequently serve as intermolecular electron−proton sources for CO_2 reduction catalyzed by **Fe-TPP**. Dihydropyridine intermediates, which can be generated by chemical or electrochemical means, can be reoxidized in air thermally or through anodic electrochemistry back to the starting nicotinamide to complete the electrochemical cycle.

A key design feature that emerges from this study is to precisely match the redox potentials of the primary-sphere molecular catalyst and second-sphere electron−proton mediator to promote productive multielectron, multiproton chemistry. For the two-electron/two-proton conversion of CO_2 to CO, catalytic rates for reduction can be augmented by up to 13.4-fold in the presence of the electron−proton mediator without sacrificing the high selectivity of **Fe-TPP** for CO_2 versus proton reduction. The cooperative second-sphere approach complements work on CO_2 hydrogenation catalysts, where metal hydrides simultaneously deliver electrons and protons.[59,83−85] Indeed, few organic hydrides are strong enough donors to reduce CO_2 directly,[73,76] and those that can be regenerated encounter slow rates of hydride transfer that limit integration into photo- or electrocatalytic cycles.[75,86] This cooperative, bioinspired approach to electrocatalysis, which leverages primary metal centers with secondary dual electron−proton reservoirs, should be applicable to a broader array of chemical transformations where bond activation and catalytic turnover rely on controlling both electron and proton inventories.

https://dx.doi.org/10.1021/acs.inorgchem.0c01162
Inorg. Chem. XXXX, XXX, XXX−XXX

■ ASSOCIATED CONTENT

Supporting Information

The Supporting Information is available free of charge at https://pubs.acs.org/doi/10.1021/acs.inorgchem.0c01162.

Experimental methods, additional electrochemistry data, and synthetic procedures (PDF)

■ AUTHOR INFORMATION

Corresponding Author

Christopher J. Chang − *Department of Chemistry and Department of Molecular and Cell Biology, University of California, Berkeley, California 94720, United States; Chemical Sciences Division, Lawrence Berkeley National Laboratory, Berkeley, California 94720, United States;* orcid.org/0000-0001-5732-9497; Email: chrischang@berkeley.edu

Authors

Peter T. Smith − *Department of Chemistry, University of California, Berkeley, California 94720, United States; Chemical Sciences Division, Lawrence Berkeley National Laboratory, Berkeley, California 94720, United States*

Sophia Weng − *Department of Chemistry, University of California, Berkeley, California 94720, United States*

Complete contact information is available at: https://pubs.acs.org/10.1021/acs.inorgchem.0c01162

Notes

The authors declare no competing financial interest.

■ ACKNOWLEDGMENTS

This work was supported by the Director, Office of Science, Office of Basic Energy Sciences, and the Division of Chemical Sciences, Geosciences, and Bioscience of the U.S. Department of Energy at Lawrence Berkeley National Laboratory (DE-AC02-05CH11231). C.J.C. is a CIFAR Senior Fellow. P.T.S. thanks the NSF for a graduate research fellowship, and S.W. thanks the UC Berkeley College of Chemistry for a summer undergraduate research award.

■ REFERENCES

(1) Kumar, B.; Llorente, M.; Froehlich, J.; Dang, T.; Sathrum, A.; Kubiak, C. P. Photochemical and Photoelectrochemical Reduction of CO_2. *Annu. Rev. Phys. Chem.* **2012**, *63* (1), 541−569.

(2) Appel, A. M.; Bercaw, J. E.; Bocarsly, A. B.; Dobbek, H.; DuBois, D. L.; Dupuis, M.; Ferry, J. G.; Fujita, E.; Hille, R.; Kenis, P. J.; Kerfeld, C. A.; Morris, R. H.; Peden, C. H.; Portis, A. R.; Ragsdale, S. W.; Rauchfuss, T. B.; Reek, J. N.; Seefeldt, L. C.; Thauer, R. K.; Waldrop, G. L. Frontiers, opportunities, and challenges in biochemical and chemical catalysis of CO_2 fixation. *Chem. Rev.* **2013**, *113* (8), 6621−6658.

(3) Costentin, C.; Robert, M.; Saveant, J.-M. Catalysis of the electrochemical reduction of carbon dioxide. *Chem. Soc. Rev.* **2013**, *42* (6), 2423−2436.

(4) Francke, R.; Schille, B.; Roemelt, M. Homogeneously Catalyzed Electroreduction of Carbon Dioxide-Methods, Mechanisms, and Catalysts. *Chem. Rev.* **2018**, *118* (9), 4631−4701.

(5) Corbin, N.; Zeng, J.; Williams, K.; Manthiram, K. Heterogeneous molecular catalysts for electrocatalytic CO_2 reduction. *Nano Res.* **2019**, *12* (9), 2093−2125.

(6) Zhang, S.; Fan, Q.; Xia, R.; Meyer, T. J. CO_2 Reduction: From Homogeneous to Heterogeneous Electrocatalysis. *Acc. Chem. Res.* **2020**, *53* (1), 255−264.

(7) De Luna, P.; Hahn, C.; Higgins, D.; Jaffer, S. A.; Jaramillo, T. F.; Sargent, E. H. What would it take for renewably powered electrosynthesis to displace petrochemical processes? *Science* **2019**, *364* (6438), No. eaav3506.

(8) Nitopi, S.; Bertheussen, E.; Scott, S. B.; Liu, X.; Engstfeld, A. K.; Horch, S.; Seger, B.; Stephens, I. E. L.; Chan, K.; Hahn, C.; Norskov, J. K.; Jaramillo, T. F.; Chorkendorff, I. Progress and Perspectives of Electrochemical CO_2 Reduction on Copper in Aqueous Electrolyte. *Chem. Rev.* **2019**, *119* (12), 7610−7672.

(9) Zhao, S.; Jin, R. X.; Jin, R. C. Opportunities and Challenges in CO_2 Reduction by Gold- and Silver-Based Electrocatalysts: From Bulk Metals to Nanoparticles and Atomically Precise Nanoclusters. *ACS Energy Lett.* **2018**, *3* (2), 452−462.

(10) Ross, M. B.; De Luna, P.; Li, Y.; Dinh, C.-T.; Kim, D.; Yang, P.; Sargent, E. H. Designing materials for electrochemical carbon dioxide recycling. *Nat. Catal.* **2019**, *2* (8), 648−658.

(11) Weekes, D. M.; Salvatore, D. A.; Reyes, A.; Huang, A.; Berlinguette, C. P. Electrolytic CO_2 Reduction in a Flow Cell. *Acc. Chem. Res.* **2018**, *51* (4), 910−918.

(12) Armstrong, F. A.; Hirst, J. Reversibility and efficiency in electrocatalytic energy conversion and lessons from enzymes. *Proc. Natl. Acad. Sci. U. S. A.* **2011**, *108* (34), 14049−14054.

(13) Kornienko, N.; Ly, K. H.; Robinson, W. E.; Heidary, N.; Zhang, J. Z.; Reisner, E. Advancing Techniques for Investigating the Enzyme-Electrode Interface. *Acc. Chem. Res.* **2019**, *52* (5), 1439−1448.

(14) Chen, H.; Dong, F.; Minteer, S. D. The progress and outlook of bioelectrocatalysis for the production of chemicals, fuels and materials. *Nat. Catal.* **2020**, *3* (3), 225−244.

(15) Smith, P. T.; Nichols, E. M.; Cao, Z.; Chang, C. J. Hybrid Catalysts for Artificial Photosynthesis: Merging Approaches from Molecular, Materials, and Biological Catalysis. *Acc. Chem. Res.* **2020**, *53* (3), 575−587.

(16) Bhugun, I.; Lexa, D.; Saveant, J.-M. Ultraefficient selective homogeneous catalysis of the electrochemical reduction of carbon dioxide by an iron(0) porphyrin associated with a weak Broensted acid cocatalyst. *J. Am. Chem. Soc.* **1994**, *116* (11), 5015−5016.

(17) Costentin, C.; Drouet, S.; Robert, M.; Saveant, J. M. A local proton source enhances CO_2 electroreduction to CO by a molecular Fe catalyst. *Science* **2012**, *338* (6103), 90−94.

(18) Costentin, C.; Passard, G.; Robert, M.; Saveant, J. M. Ultraefficient homogeneous catalyst for the CO_2-to-CO electrochemical conversion. *Proc. Natl. Acad. Sci. U. S. A.* **2014**, *111* (42), 14990−14994.

(19) Hod, I.; Sampson, M. D.; Deria, P.; Kubiak, C. P.; Farha, O. K.; Hupp, J. T. Fe-Porphyrin-Based Metal-Organic Framework Films as High-Surface Concentration, Heterogeneous Catalysts for Electrochemical Reduction of CO_2. *ACS Catal.* **2015**, *5* (11), 6302−6309.

(20) Mohamed, E. A.; Zahran, Z. N.; Naruta, Y. Efficient electrocatalytic CO_2 reduction with a molecular cofacial iron porphyrin dimer. *Chem. Commun.* **2015**, *51* (95), 16900−16903.

(21) Azcarate, I.; Costentin, C.; Robert, M.; Saveant, J. M. Through-Space Charge Interaction Substituent Effects in Molecular Catalysis Leading to the Design of the Most Efficient Catalyst of CO_2-to-CO Electrochemical Conversion. *J. Am. Chem. Soc.* **2016**, *138* (51), 16639−16644.

(22) Rao, H.; Schmidt, L. C.; Bonin, J.; Robert, M. Visible-light-driven methane formation from CO2 with a molecular iron catalyst. *Nature* **2017**, *548* (7665), 74.

(23) Smith, P. T.; Benke, B. P.; Cao, Z.; Kim, Y.; Nichols, E. M.; Kim, K.; Chang, C. J. Iron Porphyrins Embedded into a Supramolecular Porous Organic Cage for Electrochemical CO_2 Reduction in Water. *Angew. Chem., Int. Ed.* **2018**, *57* (31), 9684−9688.

(24) Mondal, B.; Sen, P.; Rana, A.; Saha, D.; Das, P.; Dey, A. Reduction of CO_2 to CO by an Iron Porphyrin Catalyst in the Presence of Oxygen. *ACS Catal.* **2019**, *9* (5), 3895−3899.

(25) Loewen, N. D.; Thompson, E. J.; Kagan, M.; Banales, C. L.; Myers, T. W.; Fettinger, J. C.; Berben, L. A. A pendant proton shuttle on $[Fe_4N(CO)_{12}]^-$ alters product selectivity in formate vs. H_2 production via the hydride $[H-Fe_4N(CO)_{12}]^-$. *Chem. Sci.* **2016**, *7* (4), 2728−2735.

(26) Roy, S.; Sharma, B.; Pecaut, J.; Simon, P.; Fontecave, M.; Tran, P. D.; Derat, E.; Artero, V. Molecular Cobalt Complexes with Pendant Amines for Selective Electrocatalytic Reduction of Carbon Dioxide to Formic Acid. *J. Am. Chem. Soc.* **2017**, *139* (10), 3685−3696.
(27) Ngo, K. T.; McKinnon, M.; Mahanti, B.; Narayanan, R.; Grills, D. C.; Ertem, M. Z.; Rochford, J. Turning on the Protonation-First Pathway for Electrocatalytic CO_2 Reduction by Manganese Bipyridyl Tricarbonyl Complexes. *J. Am. Chem. Soc.* **2017**, *139* (7), 2604−2618.
(28) Chabolla, S. A.; Machan, C. W.; Yin, J.; Dellamary, E. A.; Sahu, S.; Gianneschi, N. C.; Gilson, M. K.; Tezcan, F. A.; Kubiak, C. P. Bio-inspired CO_2 reduction by a rhenium tricarbonyl bipyridine-based catalyst appended to amino acids and peptidic platforms: incorporating proton relays and hydrogen-bonding functional groups. *Faraday Discuss.* **2017**, *198* (0), 279−300.
(29) Nichols, E. M.; Derrick, J. S.; Nistanaki, S. K.; Smith, P. T.; Chang, C. J. Positional effects of second-sphere amide pendants on electrochemical CO_2 reduction catalyzed by iron porphyrins. *Chem. Sci.* **2018**, *9* (11), 2952−2960.
(30) Margarit, C. G.; Schnedermann, C.; Asimow, N. G.; Nocera, D. G. Carbon Dioxide Reduction by Iron Hangman Porphyrins. *Organometallics* **2019**, *38* (6), 1219−1223.
(31) Chapovetsky, A.; Welborn, M.; Luna, J. M.; Haiges, R.; Miller, T. F., 3rd; Marinescu, S. C. Pendant Hydrogen-Bond Donors in Cobalt Catalysts Independently Enhance CO_2 Reduction. *ACS Cent. ACS Cent. Sci.* **2018**, *4* (3), 397−404.
(32) Haviv, E.; Azaiza-Dabbah, D.; Carmieli, R.; Avram, L.; Martin, J. M. L.; Neumann, R. A Thiourea Tether in the Second Coordination Sphere as a Binding Site for CO_2 and a Proton Donor Promotes the Electrochemical Reduction of CO_2 to CO Catalyzed by a Rhenium Bipyridine-Type Complex. *J. Am. Chem. Soc.* **2018**, *140* (39), 12451−12456.
(33) Sinha, S.; Warren, J. J. Unexpected Solvent Effect in Electrocatalytic CO_2 to CO Conversion Revealed Using Asymmetric Metalloporphyrins. *Inorg. Chem.* **2018**, *57* (20), 12650−12656.
(34) Sen, P.; Mondal, B.; Saha, D.; Rana, A.; Dey, A. Role of 2nd sphere H-bonding residues in tuning the kinetics of CO_2 reduction to CO by iron porphyrin complexes. *Dalton Trans.* **2019**, *48* (18), 5965−5977.
(35) Nichols, E. M.; Chang, C. J. Urea-Based Multipoint Hydrogen-Bond Donor Additive Promotes Electrochemical CO_2 Reduction Catalyzed by Nickel Cyclam. *Organometallics* **2019**, *38* (6), 1213−1218.
(36) Gotico, P.; Boitrel, B.; Guillot, R.; Sircoglou, M.; Quaranta, A.; Halime, Z.; Leibl, W.; Aukauloo, A. Second-Sphere Biomimetic Multipoint Hydrogen-Bonding Patterns to Boost CO_2 Reduction of Iron Porphyrins. *Angew. Chem., Int. Ed.* **2019**, *58* (14), 4504−4509.
(37) Hellman, A. N.; Haiges, R.; Marinescu, S. C. Rhenium bipyridine catalysts with hydrogen bonding pendant amines for CO_2 reduction. *Dalton Trans.* **2019**, *48* (38), 14251−14255.
(38) Zee, D. Z.; Nippe, M.; King, A. E.; Chang, C. J.; Long, J. R. Tuning Second Coordination Sphere Interactions in Polypyridyl-Iron Complexes to Achieve Selective Electrocatalytic Reduction of Carbon Dioxide to Carbon Monoxide. *Inorg. Chem.* **2020**, *59* (7), 5206−5217.
(39) Guo, K.; Li, X.; Lei, H.; Zhang, W.; Cao, R. Unexpected Effect of Intramolecular Phenolic Group on Electrocatalytic CO_2 Reduction. *ChemCatChem* **2020**, *12* (6), 1591−1595.
(40) Bhugun, I.; Lexa, D.; Savéant, J.-M. Catalysis of the Electrochemical Reduction of Carbon Dioxide by Iron(0) Porphyrins. Synergistic Effect of Lewis Acid Cations. *J. Phys. Chem.* **1996**, *100* (51), 19981−19985.
(41) Sampson, M. D.; Kubiak, C. P. Manganese Electrocatalysts with Bulky Bipyridine Ligands: Utilizing Lewis Acids To Promote Carbon Dioxide Reduction at Low Overpotentials. *J. Am. Chem. Soc.* **2016**, *138* (4), 1386−1393.
(42) Hong, D.; Kawanishi, T.; Tsukakoshi, Y.; Kotani, H.; Ishizuka, T.; Kojima, T. Efficient Photocatalytic CO_2 Reduction by a Ni(II) Complex Having Pyridine Pendants through Capturing a Mg^{2+} Ion as a Lewis-Acid Cocatalyst. *J. Am. Chem. Soc.* **2019**, *141*, 20309.
(43) Wang, M.; Torbensen, K.; Salvatore, D.; Ren, S.; Joulié, D.; Dumoulin, F.; Mendoza, D.; Lassalle-Kaiser, B.; Işci, U.; Berlinguette, C. P.; Robert, M. CO_2 electrochemical catalytic reduction with a highly active cobalt phthalocyanine. *Nat. Commun.* **2019**, *10* (1), 3602.
(44) Sung, S.; Kumar, D.; Gil-Sepulcre, M.; Nippe, M. Electrocatalytic CO_2 Reduction by Imidazolium-Functionalized Molecular Catalysts. *J. Am. Chem. Soc.* **2017**, *139* (40), 13993−13996.
(45) Khadhraoui, A.; Gotico, P.; Boitrel, B.; Leibl, W.; Halime, Z.; Aukauloo, A. Local ionic liquid environment at a modified iron porphyrin catalyst enhances the electrocatalytic performance of CO_2 to CO reduction in water. *Chem. Commun.* **2018**, *54* (82), 11630−11633.
(46) Sung, S.; Li, X.; Wolf, L. M.; Meeder, J. R.; Bhuvanesh, N. S.; Grice, K. A.; Panetier, J. A.; Nippe, M. Synergistic Effects of Imidazolium-Functionalization on fac-$Mn(CO)_3$ Bipyridine Catalyst Platforms for Electrocatalytic Carbon Dioxide Reduction. *J. Am. Chem. Soc.* **2019**, *141* (16), 6569−6582.
(47) Schneider, C. R.; Shafaat, H. S. An internal electron reservoir enhances catalytic CO_2 reduction by a semisynthetic enzyme. *Chem. Commun.* **2016**, *52* (64), 9889−9892.
(48) Lin, S.; Diercks, C. S.; Zhang, Y. B.; Kornienko, N.; Nichols, E. M.; Zhao, Y.; Paris, A. R.; Kim, D.; Yang, P.; Yaghi, O. M.; Chang, C. J. Covalent organic frameworks comprising cobalt porphyrins for catalytic CO_2 reduction in water. *Science* **2015**, *349* (6253), 1208−1213.
(49) Diercks, C. S.; Lin, S.; Kornienko, N.; Kapustin, E. A.; Nichols, E. M.; Zhu, C.; Zhao, Y.; Chang, C. J.; Yaghi, O. M. Reticular Electronic Tuning of Porphyrin Active Sites in Covalent Organic Frameworks for Electrocatalytic Carbon Dioxide Reduction. *J. Am. Chem. Soc.* **2018**, *140* (3), 1116−1122.
(50) Chen, Z.; Chen, C.; Weinberg, D. R.; Kang, P.; Concepcion, J. J.; Harrison, D. P.; Brookhart, M. S.; Meyer, T. J. Electrocatalytic reduction of CO_2 to CO by polypyridyl ruthenium complexes. *Chem. Commun.* **2011**, *47* (47), 12607−12609.
(51) Benson, E. E.; Sampson, M. D.; Grice, K. A.; Smieja, J. M.; Froehlich, J. D.; Friebel, D.; Keith, J. A.; Carter, E. A.; Nilsson, A.; Kubiak, C. P. The Electronic States of Rhenium Bipyridyl Electrocatalysts for CO_2 Reduction as Revealed by X-ray Absorption Spectroscopy and Computational Quantum Chemistry. *Angew. Chem., Int. Ed.* **2013**, *52* (18), 4841−4844.
(52) Elgrishi, N.; Chambers, M. B.; Artero, V.; Fontecave, M. Terpyridine complexes of first row transition metals and electrochemical reduction of CO_2 to CO. *Phys. Chem. Chem. Phys.* **2014**, *16* (27), 13635−13644.
(53) Gonell, S.; Massey, M. D.; Moseley, I. P.; Schauer, C. K.; Muckerman, J. T.; Miller, A. J. M. The Trans Effect in Electrocatalytic CO_2 Reduction: Mechanistic Studies of Asymmetric Ruthenium Pyridyl-Carbene Catalysts. *J. Am. Chem. Soc.* **2019**, *141* (16), 6658−6671.
(54) Derrick, J.; Loipersberger, M.; Iovan, D.; Smith, P. T.; Chakarawet, K.; Long, J. R.; Head-Gordon, M.; Chang, C. Metal−Ligand Exchange Coupling Promotes Iron-Catalyzed Electrochemical CO_2 Reduction at Low Overpotentials. *ChemRxiv* **2020**. DOI: 10.26434/chemrxiv.11923176.v1.
(55) Gonell, S.; Lloret, J.; Miller, A. An Iron Pyridyl-Carbene Catalyst for Low Overpotential CO_2 reduction to CO: Mechanistic Comparisons with the Ruthenium Analogue and Photochemical Promotion. *ChemRxiv* **2020**. DOI: 10.26434/chemrxiv.11911383.v1.
(56) Lacy, D. C.; McCrory, C. C. L.; Peters, J. C. Studies of Cobalt-Mediated Electrocatalytic CO_2 Reduction Using a Redox-Active Ligand. *Inorg. Chem.* **2014**, *53* (10), 4980−4988.
(57) Romelt, C.; Song, J.; Tarrago, M.; Rees, J. A.; van Gastel, M.; Weyhermuller, T.; DeBeer, S.; Bill, E.; Neese, F.; Ye, S. Electronic Structure of a Formal Iron(0) Porphyrin Complex Relevant to CO_2 Reduction. *Inorg. Chem.* **2017**, *56* (8), 4745−4751.
(58) Wu, Y.; Jiang, J.; Weng, Z.; Wang, M.; Broere, D. L. J.; Zhong, Y.; Brudvig, G. W.; Feng, Z.; Wang, H. Electroreduction of CO_2

Catalyzed by a Heterogenized Zn-Porphyrin Complex with a Redox-Innocent Metal Center. *ACS Cent. Sci.* **2017**, *3* (8), 847−852.
(59) Ceballos, B. M.; Yang, J. Y. Directing the reactivity of metal hydrides for selective CO_2 reduction. *Proc. Natl. Acad. Sci. U. S. A.* **2018**, *115* (50), 12686−12691.
(60) Su, X.; McCardle, K. M.; Panetier, J. A.; Jurss, J. W. Electrocatalytic CO_2 reduction with nickel complexes supported by tunable bipyridyl-N-heterocyclic carbene donors: understanding redox-active macrocycles. *Chem. Commun.* **2018**, *54* (27), 3351−3354.
(61) Maurin, A.; Robert, M. Noncovalent Immobilization of a Molecular Iron-Based Electrocatalyst on Carbon Electrodes for Selective, Efficient CO_2-to-CO Conversion in Water. *J. Am. Chem. Soc.* **2016**, *138* (8), 2492−2495.
(62) Oh, S.; Gallagher, J. R.; Miller, J. T.; Surendranath, Y. Graphite-Conjugated Rhenium Catalysts for Carbon Dioxide Reduction. *J. Am. Chem. Soc.* **2016**, *138* (6), 1820−1823.
(63) Hu, X. M.; Ronne, M. H.; Pedersen, S. U.; Skrydstrup, T.; Daasbjerg, K. Enhanced Catalytic Activity of Cobalt Porphyrin in CO_2 Electroreduction upon Immobilization on Carbon Materials. *Angew. Chem., Int. Ed.* **2017**, *56* (23), 6468−6472.
(64) Wang, M.; Chen, L.; Lau, T. C.; Robert, M. A Hybrid Co Quaterpyridine Complex/Carbon Nanotube Catalytic Material for CO_2 Reduction in Water. *Angew. Chem., Int. Ed.* **2018**, *57* (26), 7769−7773.
(65) Zhanaidarova, A.; Jones, S. C.; Despagnet-Ayoub, E.; Pimentel, B. R.; Kubiak, C. P. Re(tBu-bpy)$(CO)_3$Cl Supported on Multi-Walled Carbon Nanotubes Selectively Reduces CO_2 in Water. *J. Am. Chem. Soc.* **2019**, *141* (43), 17270−17277.
(66) Jeoung, J. H.; Dobbek, H. Carbon dioxide activation at the Ni,Fe-cluster of anaerobic carbon monoxide dehydrogenase. *Science* **2007**, *318* (5855), 1461−1464.
(67) Boyington, J. C.; Gladyshev, V. N.; Khangulov, S. V.; Stadtman, T. C.; Sun, P. D. Crystal Structure of Formate Dehydrogenase H: Catalysis Involving Mo, Molybdopterin, Selenocysteine, and an Fe_4S_4 Cluster. *Science* **1997**, *275* (5304), 1305−1308.
(68) Parkin, A.; Seravalli, J.; Vincent, K. A.; Ragsdale, S. W.; Armstrong, F. A. Rapid and efficient electrocatalytic CO_2/CO interconversions by Carboxydothermus hydrogenoformans CO dehydrogenase I on an electrode. *J. Am. Chem. Soc.* **2007**, *129* (34), 10328−10329.
(69) Reda, T.; Plugge, C. M.; Abram, N. J.; Hirst, J. Reversible interconversion of carbon dioxide and formate by an electroactive enzyme. *Proc. Natl. Acad. Sci. U. S. A.* **2008**, *105* (31), 10654−10658.
(70) Fourmond, V.; Léger, C. Protein Electrochemistry: Questions and Answers. *Adv. Biochem. Eng./Biotechnol.* **2016**, *158*, 1−41.
(71) Yates, N. D. J.; Fascione, M. A.; Parkin, A. Methodologies for "Wiring" Redox Proteins/Enzymes to Electrode Surfaces. *Chem. - Eur. J.* **2018**, *24* (47), 12164−12182.
(72) Ilic, S.; Alherz, A.; Musgrave, C. B.; Glusac, K. D. Importance of proton-coupled electron transfer in cathodic regeneration of organic hydrides. *Chem. Commun.* **2019**, *55* (39), 5583−5586.
(73) McSkimming, A.; Colbran, S. B. The coordination chemistry of organo-hydride donors: new prospects for efficient multi-electron reduction. *Chem. Soc. Rev.* **2013**, *42* (12), 5439−5488.
(74) Costentin, C. Electrochemical approach to the mechanistic study of proton-coupled electron transfer. *Chem. Rev.* **2008**, *108* (7), 2145−2179.
(75) Lim, C. H.; Ilic, S.; Alherz, A.; Worrell, B. T.; Bacon, S. S.; Hynes, J. T.; Glusac, K. D.; Musgrave, C. B. Benzimidazoles as Metal-Free and Recyclable Hydrides for CO_2 Reduction to Formate. *J. Am. Chem. Soc.* **2019**, *141* (1), 272−280.
(76) Ilic, S.; Alherz, A.; Musgrave, C. B.; Glusac, K. D. Thermodynamic and kinetic hydricities of metal-free hydrides. *Chem. Soc. Rev.* **2018**, *47* (8), 2809−2836.
(77) Margolis, S. A.; Howell, B. F.; Schaffer, R. Purification and analysis of the purity of NADH. *Clin. Chem.* **1976**, *22* (8), 1322−1329.
(78) Lim, C. H.; Holder, A. M.; Hynes, J. T.; Musgrave, C. B. Reduction of CO_2 to methanol catalyzed by a biomimetic organo-hydride produced from pyridine. *J. Am. Chem. Soc.* **2014**, *136* (45), 16081−16095.
(79) Anson, C. W.; Stahl, S. S. Cooperative Electrocatalytic O_2 Reduction Involving Co(salophen) with p-Hydroquinone as an Electron-Proton Transfer Mediator. *J. Am. Chem. Soc.* **2017**, *139* (51), 18472−18475.
(80) Wang, F.; Stahl, S. S. Electrochemical Oxidation of Organic Molecules at Lower Overpotential: Accessing Broader Functional Group Compatibility with Electron−Proton Transfer Mediators. *Acc. Chem. Res.* **2020**, *53* (3), 561−574.
(81) Costentin, C.; Drouet, S.; Robert, M.; Saveant, J. M. Turnover numbers, turnover frequencies, and overpotential in molecular catalysis of electrochemical reactions. Cyclic voltammetry and preparative-scale electrolysis. *J. Am. J. Am. Chem. Soc.* **2012**, *134* (27), 11235−11242.
(82) Liu, Y.; McCrory, C. C. L. Modulating the mechanism of electrocatalytic CO_2 reduction by cobalt phthalocyanine through polymer coordination and encapsulation. *Nat. Commun.* **2019**, *10* (1), 1683.
(83) Kang, P.; Cheng, C.; Chen, Z.; Schauer, C. K.; Meyer, T. J.; Brookhart, M. Selective Electrocatalytic Reduction of CO_2 to Formate by Water-Stable Iridium Dihydride Pincer Complexes. *J. Am. Chem. Soc.* **2012**, *134* (12), 5500−5503.
(84) Taheri, A.; Thompson, E. J.; Fettinger, J. C.; Berben, L. A. An Iron Electrocatalyst for Selective Reduction of CO_2 to Formate in Water: Including Thermochemical Insights. *ACS Catal.* **2015**, *5* (12), 7140−7151.
(85) Waldie, K. M.; Ostericher, A. L.; Reineke, M. H.; Sasayama, A. F.; Kubiak, C. P. Hydricity of Transition-Metal Hydrides: Thermodynamic Considerations for CO_2 Reduction. *ACS Catal.* **2018**, *8* (2), 1313−1324.
(86) Ohtsu, H.; Tanaka, K. An organic hydride transfer reaction of a ruthenium NAD model complex leading to carbon dioxide reduction. *Angew. Chem., Int. Ed.* **2012**, *51* (39), 9792−9795.

https://dx.doi.org/10.1021/acs.inorgchem.0c01162
Inorg. Chem. XXXX, XXX, XXX−XXX